

Design of photonic band gap nanocavities for stimulated Raman amplification and lasing in monolithic silicon

Xiaodong Yang and Chee Wei Wong

Optical Nanostructures Laboratory, Columbia University
New York, NY 10027 USA

xy2103@columbia.edu, cww2104@columbia.edu

Abstract: The concept and design of $L5$ photonic band gap nanocavities in two-dimensional photonic crystal slabs for enhancement of stimulated Raman amplification and lasing in monolithic silicon is suggested for the first time. Specific high quality factor and small modal volume nanocavities are designed which supports the required pump-Stokes modal spacing in silicon, with ultralow lasing thresholds.

©2005 Optical Society of America

OCIS codes: (190.4390) Nonlinear optics, integrated optics; (230.5750) Resonators; (140.3550) Lasers, Raman; (140.5960) Semiconductor lasers; (230.3990) Microstructure devices.

References and links

1. L. Pavesi and D. J. Lockwood, *Silicon Photonics*, (Springer-verlag, New York, 2004); G. T. Reed and A. P. Knights, *Silicon Photonics: An Introduction* (John Wiley, West Sussex, 2004).
2. K. Wada, K., H. C. Luan, D. R. C. Lim and L. C. Kimerling., "On-chip interconnection beyond semiconductor roadmap: silicon microphotonics," Proc. SPIE **4870**, 437-443 (2002).
3. V. R. Almeida, C. A. Barrios, R. R. Panepucci and M. Lipson, "All-optical control of light on a silicon chip," Nature **431**, 1081-1084 (2004); V. R. Almeida and M. Lipson, "Optical bistability on a silicon chip," Opt. Letters **29**, 2387-2389 (2004).
4. R. Claps, D. Dimitropoulos, V. Raghunathan, Y. Han, and B. Jalali, "Observation of stimulated Raman amplification in silicon waveguides," Opt. Express **11**, 1731-1739 (2003), <http://www.opticsexpress.org/abstract.cfm?URI=OPEX-11-15-1731>
5. R. L. Espinola, J. I. Dadap, R. M. Osgood, Jr., S. J. McNab, and Y. A. Vlasov, "Raman amplification in ultrasmall silicon-on-insulator wire waveguides," Opt. Express **12**, 3713 - 3718 (2004), <http://www.opticsexpress.org/abstract.cfm?URI=OPEX-12-16-3713>
6. T. K. Liang and H. K. Tsang, "Efficient Raman amplification in silicon-on-insulator waveguides," Appl. Phys. Lett. **85**, 3343-3345 (2004).
7. A. Liu, H. Rong, M. Paniccia, O. Cohen, and D. Hak, "Net optical gain in a low loss silicon-on-insulator waveguide by stimulated Raman scattering," Opt. Express **12**, 4261-4268 (2004), <http://www.opticsexpress.org/abstract.cfm?URI=OPEX-12-18-4261>
8. Q. Xu, V. R. Almeida, and M. Lipson, "Time-resolved study of Raman gain in highly confined silicon-on-insulator waveguides," Opt. Express **12**, 4437 - 4442 (2004), <http://www.opticsexpress.org/abstract.cfm?URI=OPEX-12-19-4437>
9. O. Boyraz and B. Jalali, "Demonstration of a silicon Raman laser," Opt. Express **12**, 5269-5273 (2004), <http://www.opticsexpress.org/abstract.cfm?URI=OPEX-12-21-5269>
10. R. Jones, H. Rong, A. Liu, A. W. Fang, M. J. Paniccia, D. Hak, and O. Cohen, "Net continuous wave optical gain in a low loss silicon-on-insulator waveguide by stimulated Raman scattering," Opt. Express **13**, 519-525 (2005), <http://www.opticsexpress.org/abstract.cfm?URI=OPEX-13-2-519>; H. Rong, A. Liu, R. Jones, O. Cohen, D. Hak, R. Nicolaescu, A. Fang and M. Paniccia, "An all-silicon Raman laser," Nature **433**, 292-294 (2005); H. Rong, R. Jones, A. Liu, O. Cohen, D. Hak, A. Fang and M. Paniccia, "A continuous-wave Raman silicon laser," Nature **433**, 725-728 (2005).
11. O. Boyraz and B. Jalali, "Demonstration of directly modulated silicon Raman laser," Opt. Express **13**, 796-800 (2005), <http://www.opticsexpress.org/abstract.cfm?URI=OPEX-13-3-796>
12. R. Jones, A. Liu, H. Rong, M. Paniccia, O. Cohen, and D. Hak, "Lossless optical modulation in a silicon waveguide using stimulated Raman scattering," Opt. Express **13**, 1716-1723 (2005), <http://www.opticsexpress.org/abstract.cfm?URI=OPEX-13-5-1716>
13. K. Srinivasan and O. Painter, "Momentum space design of high-Q photonic crystal optical cavities," Opt. Express **10**, 670-684 (2002), <http://www.opticsexpress.org/abstract.cfm?URI=OPEX-10-15-670>

14. Y. Akahane, T. Asano, B. S. Song, and S. Noda, "High-Q photonic nanocavity in a two-dimensional photonic crystal," *Nature* **425**, 944-947 (2003).
15. H. Ryu, M. Notomi, G. Kim, and Y. Lee, "High quality-factor whispering-gallery mode in the photonic crystal hexagonal disk cavity," *Opt. Express* **12**, 1708-1719 (2004), <http://www.opticsexpress.org/abstract.cfm?URI=OPEX-12-8-1708>
16. Z. Zhang and M. Qiu, "Small-volume waveguide-section high Q microcavities in 2D photonic crystal slabs," *Opt. Express* **12**, 3988-3995 (2004), <http://www.opticsexpress.org/abstract.cfm?URI=OPEX-12-17-3988>
17. B. S. Song, S. Noda, T. Asano, and Y. Akahane, "Ultra-high-Q photonic double-heterostructure nanocavity," *Nature Materials* **4**, 207-210 (2005); B. S. Song, S. Noda, and T. Asano, "Photonic devices based on in-plane hetero photonic crystals," *Science* **300**, 1537 (2003).
18. P. Koonath, T. Indukuri, and B. Jalali, "Vertically-coupled microdisk resonators realized using three-dimensional sculpting in silicon," *Appl. Phys. Lett.* **85**, 1018-1020 (2003).
19. M. Borselli, K. Srinivasan, P. E. Barclay, and O. Painter, "Rayleigh scattering, mode coupling, and optical loss in silicon microdisks," *Appl. Phys. Lett.* **85**, 3693-3695 (2004).
20. K. J. Vahala, "Optical microcavities," *Nature* **424**, 839-846 (2003).
21. H. G. Park, S. H. Kim, S. H. Kwon, Y. G. Ju, J. K. Yang, J. H. Baek, S. B. Kim, and Y. H. Lee, "Electrically driven single-cell photonic crystal laser," *Science* **305**, 1444-1447(2004).
22. T. Yoshie, A. Scherer, J. Hendrickson, G. Khitrova, H. M. Gibbs, G. Rupper, C. Ell, O. B. Shchekin, and D. G. Deppe, "Vacuum Rabi splitting with a single quantum dot in a photonic crystal nanocavity," *Nature* **432**, 200-203 (2004).
23. M. Soljacic, and J. D. Joannopoulos, "Enhancement of nonlinear effects using photonic crystals," *Nature materials* **3**, 211-219 (2004).
24. J. Scheuer, G. T. Paloczi, J. K. S. Poon, and A. Yariv, "Coupled resonator optical waveguides: toward the slowing and storage of light," *Optics & Photonics News* **16** (2), 36-40, (2005).
25. P. E. Barclay, K. Srinivasan, and O. Painter, "Nonlinear response of silicon photonic crystal microresonators excited via an integrated waveguide and fiber taper," *Opt. Express* **13**, 801-820 (2005), <http://www.opticsexpress.org/abstract.cfm?URI=OPEX-13-3-801>
26. M. Notomi, A. Shinya, S. Mitsugi, G. Kira, E. Kuramochi, and T. Tanabe, "Optical bistable switching action of Si high-Q photonic-crystal nanocavities," *Opt. Express* **13**, 2678-2687 (2005), <http://www.opticsexpress.org/abstract.cfm?URI=OPEX-13-7-2678>
27. M. Spillane, T. J. Kippenberg, and K. J. Vahala, "Ultralow-threshold Raman laser using a spherical dielectric microcavity," *Nature* **415**, 621-623 (2002).
28. T. J. Kippenberg, S. M. Spillane, D. K. Armani, and K. J. Vahala, "Ultralow-threshold microcavity Raman laser on a microelectronic chip," *Optics Letters* **29**, 1224-1226 (2004).
29. H. K. Tsang, C. S. Wong, T. K. Liang, I. E. Day, S. W. Roberts, A. Harpin, J. Drake, and M. Asghari, "Optical dispersion, two-photon absorption and self-phase modulation in silicon waveguides at 1.5 μm wavelength," *Appl. Phys. Lett.* **80**, 416-418 (2002).
30. X. Yang, J. Yan, and C. W. Wong, "Design and fabrication of L5 photonic band gap nanocavities for stimulated Raman amplification in monolithic silicon," *CLEO/QELS*, CMU2, Baltimore, Maryland (2005).
31. Y. R. Shen, *The Principles of Nonlinear Optics*, (Wiley, Hoboken, New Jersey, 2003); Y. R. Shen and N. Bloembergen, "Theory of stimulated Brillouin and Raman scattering," *Phys. Rev.* **137** (6A), A1787 (1965).
32. F. X. Kärtner, D. J. Dougherty, H. A. Haus, E. P. Ippen, "Raman noise and soliton squeezing," *J. Opt. Soc. Am. B.* **11**, 1267 (1994); R. H. Stolen, J. P. Gordon, W. J. Tomlinson, and H. A. Haus, "Raman response function of silica-core fibers," *J. Opt. Soc. Am. B.* **6**, 1159 (1989).
33. K. J. Blow and D. Wood, "Theoretical description of transient stimulated Raman scattering in optical fibers," *IEEE J. Quan. Elect.* **25**, 2665 (1989).
34. A. Höök, "Influence of stimulated Raman scattering on cross-phase modulation between waves in optical fibers," *Opt. Lett.* **17**, 115 (1992).
35. E. Golovchenko, P. V. Mamyshv, A. N. Pilipetskii, and E. M. Dianov, "Mutual influence of the parametric effects and stimulated Raman scattering in optical fibers," *IEEE J. of Quan. Elect.* **26** (10), 1815 (1990).
36. R. G. Zaporozhchenko, S. Ya. Kilin, A. G. Smirnov, "Stimulated Raman scattering of light in a photonic crystal," *Quan. Elect.* **30**, 997 (2000).
37. X. Chen, Nicolae C. Panou, and R. M. Osgood, Jr., Microelectronics Sciences Laboratories, Columbia University, New York, NY 10027, (personal communication, 2005).
38. V. E. Perlin and H. G. Winful, "Stimulated Raman Scattering in nonlinear periodic structures," *Phys. Rev. A* **64**, 043804 (2001); H. G. Winful, V. E. Perlin, and M. Franke, "Stimulated Raman and Brillouin Scattering in nonlinear periodic structures," in *Proc. of Nonlinear Optics: Materials, Fundamentals, and Applications*, Kaua'i-Lihue, Hawaii (2000).
39. M. Krause, H. Renner, and E. Brinkmeyer, "Analysis of Raman lasing characteristics in silicon-on-insulator waveguides," *Opt. Express* **12**, 5703-5710 (2004), <http://www.opticsexpress.org/abstract.cfm?URI=OPEX-12-23-5703>
40. C. Sauvan, P. Lalanne, and J.P. Hugonin, "Slow-wave effect and mode-profile matching in Photonic Crystal microcavities," *Phys. Rev. B* (to be published), <http://arxiv.org/abs/cond-mat/0502664> .

41. A. B. Matsko, A. A. Savchenkov, R. J. Letargat, V. S. Ilchenko, and L. Maleki, "On cavity modification of stimulated Raman scattering," *J. Opt. B: Quantum Semiclass. Opt.* **5**, 272-278 (2003).
42. H.-B. Lin and A. J. Campillo, "cw nonlinear optics in droplet microcavities displaying enhanced gain," *Phys. Rev. Lett.* **73**, 2440 (1994); H.-B. Lin and A. J. Campillo, "Microcavity enhanced Raman gain," *Opt. Comm.* **133**, 287 (1997).
43. H. Yokoyama and S. D. Brorson, "Rate equation analysis of microcavity lasers," *J. Appl. Phys.* **66** (10), 4801 (1989).
44. H. M. Lai, P. T. Leung, K. Young, "Electromagnetic decay into a narrow resonance in an optical cavity," *Phys. Rev. A.* **37**, 1597 (1988).
45. B. Min, T. J. Kippenberg, and K. J. Vahala, "Compact, fiber-compatible, cascaded Raman laser," *Optics Lett.* **28** (17), 1507 (2003).
46. Y. Wu, X. Yang, and P. T. Leung, "Theory of microcavity-enhanced Raman gain," *Opt. Lett.* **24**, 345 (1999); Y. Wu and P. T. Leung, "Lasing threshold for whispering-gallery-mode microsphere lasers," *Phys. Rev. A* **60**, 630 (1999).
47. For a one-dimensional cavity, the enhancement reduces to the Yokoyama-Brorson factor (Ref. [43]) as suggested in Ref. [46].
48. S. G. Johnson and J. D. Joannopoulos, "Block-iterative frequency-domain methods for Maxwell's equations in a planewave basis," *Opt. Express* **8**, 173-190 (2001), <http://www.opticsexpress.org/abstract.cfm?URI=OPEX-8-3-173>
49. A. Taflov and S. Hagness, *Computational Electrodynamics: The Finite-Difference Time-Domain Method* (Artech House Publishers, 2000); *RSoft FullWave* commercial software used.
50. S. G. Johnson, MIT, Cambridge, MA, personal communication, 2005; V. A. Mandelshtam and H. S. Taylor, "Harmonic inversion of time signals," *J. Chem. Phys.* **107**, 6756 (1997); Erratum, *ibid.* **109**, 4128 (1998).

1. Introduction

Silicon is increasingly being considered as a dominant platform for photonic integrated circuits, which can be integrated with silicon CMOS electronics [1,2]. Subwavelength passive silicon photonic devices such as bends, splitters, and filters have been developed. Recently, with strong light confinement in silicon microstructures such as planar waveguides and microring resonators, nonlinear optical properties in silicon are enhanced and active functionalities in highly integrated silicon devices have been realized, such as all-optical switches with two-photon absorption and the thermal-optic effect [3], and all-silicon Raman amplification and lasing [4-12].

Two-dimensional (2D) photonic crystal (PhC) slabs are widely used for optical applications as they can confine light by the photonic band gap effect in plane with the aid of total internal reflection vertically. Introduction of point and line defects into 2D PhC slabs create nanocavities and PhC waveguides with arbitrary dispersion control. Through k -space design of cavity modes [13], remarkable high- Q/V_m nanocavities [14-17] have been achieved. High- Q silicon microdisks have also been recently reported [18,19]. The strong light confinement and light-matter interactions in these cavities permit fundamental studies and integrated nanophotonics applications [20], such as channel add/drop filters, low-threshold quantum well lasers [21], cavity quantum electrodynamics [22], enhancement of optical nonlinearities [23], slow light in coupled resonator optical waveguides [24], and ultrasmall nonlinear bistable devices [25,26].

Concurrently, recent work on silica-based high- Q microcavities have shown remarkable ultra-low threshold Raman lasing in silica microspheres [27] and silica microdisks [28]. Light generation and amplification through stimulated Raman scattering (SRS) in planar silicon waveguides have been observed recently [4-8], where the bulk Raman gain coefficient g_R is 10^3 to 10^4 times higher in silicon than in silica with a correspondingly narrower gain bandwidth. In particular, Raman lasing using silicon waveguides as the gain medium was recently demonstrated [9-12]. Two-photon absorption induced free-carrier absorption [29] is addressed using pulsed operation or reversed biased p-i-n diodes. These elements can be directly integrated onto CMOS-compatible silicon chips.

To achieve significant amplification and ultimately lasing, the gain medium should be placed in a cavity to achieve low thresholds or minimization of device footprints on a silicon chip: the challenge becomes achieving and designing sufficiently high- Q cavities with small modal volumes V_m . Here we suggest, for the first time, the enhanced stimulated Raman amplification and ultralow threshold Raman lasing possible in high- Q/V_m photonic band gap nanocavities [30]. This permits applications such as wavelength-selectable signal amplification and lasing in monolithic silicon for subwavelength photonic integrated circuits, novel nanocavity-based lasers at new wavelengths, and further facilitates and advances the study of nonlinear phenomena at small lengthscales. As a specific example, we will illustrate designs of a particular $L5$ photonic band gap nanocavities for enhanced SRS and Raman lasing, in which lasing thresholds on order of tens to hundreds of μW can be achieved.

2. Design concept and theoretical background

Stimulated Raman scattering is an inelastic two-photon process, where an incident photon interacts with an excited state of the material (the LO and TO phonons of single-crystal silicon in our case). The strongest Stokes peak arises from single first-order Raman phonon (three-fold degenerate) at the Brillouin zone center. Coupling between the pump and Stokes waves in SRS can be understood classically with nonlinear polarizations $\mathbf{P}^{(3)}$, where $\mathbf{P}^{(3)}$ is $\chi_{jkmn}^{(3)} \mathbf{E}_p \mathbf{E}_p^* \mathbf{E}_s$, $\chi_{jkmn}^{(3)}$ the third-order fourth-rank Raman susceptibility, and \mathbf{E}_p and \mathbf{E}_s the electric fields of the pump and Stokes waves respectively. The dynamics of SRS is governed through a set of time-dependent coupled nonlinear equations [31]. Interaction of the Raman effect for ultrashort pulses, including contribution to the Kerr effect, has been carefully studied [32-33]. Here we employ the slowly varying envelope approximation for the forward and backward propagation pump wave amplitudes A_p^\pm and Stokes wave amplitudes A_s^\pm . The coupled nonlinear equations have been explored [34-37] and in particular described by Perlin *et al.* [38] and Krause *et al.* [39] as:

$$\pm \frac{\partial A_p^\pm}{\partial z} + \frac{1}{v_p} \frac{\partial A_p^\pm}{\partial t} = \left\{ -\frac{g_p}{2} (|A_s^+|^2 + |A_s^-|^2) + i\gamma_p [|A_p^\pm|^2 + 2(|A_p^\mp|^2 + |A_s^+|^2 + |A_s^-|^2)] - \frac{\alpha_p}{2} \right. \\ \left. - \beta [|A_p^\pm|^2 + 2(|A_p^\mp|^2 + |A_s^+|^2 + |A_s^-|^2)] - \bar{\varphi} \lambda_p^2 \bar{N}_{eff} \right\} A_p^\pm \quad (1)$$

$$\pm \frac{\partial A_s^\pm}{\partial z} + \frac{1}{v_s} \frac{\partial A_s^\pm}{\partial t} = \left\{ \frac{g_s}{2} (|A_p^+|^2 + |A_p^-|^2) + i\gamma_s [|A_s^\pm|^2 + 2(|A_s^\mp|^2 + |A_p^+|^2 + |A_p^-|^2)] - \frac{\alpha_s}{2} \right. \\ \left. - \beta [|A_s^\pm|^2 + 2(|A_s^\mp|^2 + |A_p^+|^2 + |A_p^-|^2)] - \bar{\varphi} \lambda_s^2 \bar{N}_{eff} \right\} A_s^\pm \\ + i\kappa A_s^\mp + i\delta\beta A_s^\pm \quad (2)$$

Here material dispersion is considered negligible compared to the cavity dispersion, and only the 1st order Stokes is considered. The first two terms on the right-hand side represent SRS and Kerr nonlinearities respectively, with $g_{p,s}$ the Raman gain coefficients at the pump and Stokes frequencies (reported in silicon $\sim 20 - 76 \text{ cm/GW}$ [39] at the C-band) and $\gamma_{p,s}$ the Kerr nonlinear coefficients ($= 2\pi n_2/\lambda_{p,s}$) at the pump and Stokes frequencies. In the Kerr term, the $2|A_j|^2 A_k$ terms represent cross-phase modulation while the $|A_j|^2 A_k$ terms represent self-phase modulation. $v_{p,s}$ are the respective group velocities for the pump and Stokes waves. The α -terms account for linear loss, the κ -terms account for forward and backward coupling, and the $\delta\beta$ -terms account for signal detuning from Bragg resonance. β is the two-photon absorption (TPA) coefficient of silicon, $\bar{\varphi}$ the efficiency of the free-carrier absorption (FCA) process,

and \bar{N}_{eff} the effective charge-carrier density. A full discussion of this framework for periodic structures can be found in the reference 38. The above coupled equations can be employed for continuous-wave or pulsed operations. The effective $A_{p,s}^{\pm}$ can be calculated inside high- Q/V_m nanocavities through a Fabry-Perot model [40].

Classical field accumulation of both $|A_s|^2$ and $|A_p|^2$ intensities, as seen in Equations (1) and (2), within a cavity enhances the spontaneous and stimulated Raman scattering process, since the Raman gain coefficient is intensity dependent. For laser oscillation, the gain condition requires the round-trip gain G_R to exceed the round-trip loss α for initiation of oscillation: $(G_R - \alpha) > 0$. The power build up in a cavity has a Q/V_m dependence, while the cavity round-trip loss has a $1/Q$ dependence from the definition of Q . Equating G_R with α , the lasing threshold $P_{threshold}$ can thus be described by:

$$P_{threshold} = \frac{\pi^2 n_s n_p}{g_s \xi \lambda_s \lambda_p} \frac{V_m}{Q_s Q_p} \quad (3)$$

where V_m is the effective modal volume, ξ the modal overlap, $Q_{p,s}$ the cavity quality factors, $n_{p,s}$ the refractive indices at the pump and Stokes wavelengths λ_p and λ_s respectively. Both the pump and Stokes in the nanocavity are designed to have the same (e.g. even) symmetry to maximize the overlap ξ between the modes. The character of this threshold is similar to that derived for whispering gallery modes in microspheres and microcavities [27, 28, 41]. Note that in this classical formulation, the Raman gain coefficient g_s is still equivalent to the bulk Raman gain efficient g_b , without considerations of possible cavity quantum electrodynamics (QED) enhancements.

The lasing threshold scales with $V_m/Q_s Q_p$ as illustrated in Equation (3). This therefore suggests the motivation for small V_m cavities with high- Q factors. In fact, for microscopic spherical cavities (with $\sim 70 \mu\text{m}$ radius) where V_m has an approximate quadratic dependence on the lengthscale R , a R^2 dependence for the Raman lasing threshold has been observed experimentally [27]. For even smaller spherical microdroplets (with $\sim 4 \mu\text{m}$ radius), a stronger R^4 dependence on the Raman lasing threshold has been observed experimentally [42]. This additional R^2 dependence in the microdroplets is attributed to cavity QED enhancements, particularly when the cavity linewidths are significantly smaller than the homogenous linewidth of the scattering process (when Fermi's golden rule breaks down). Here the gain coefficient g_s should be the Raman gain in a cavity g_c , which can be approximated by the ratio of the density of states with the cavity compared to that of free space and looking only at the transition rate per mode [43, 44]. Even without considering these cavity QED enhancements and considering only classical local field enhancement, *the Raman lasing threshold in silicon photonic band gap nanocavities can be estimated through Equation (3) to be on order tens to hundreds of μW* , based on the high- Q/V_m nanocavities to be described in following section.

Analysis of the possible cavity enhancement of the Raman gain coefficient g_c is explored by several groups [27, 42, 45, 46]. For example, Wu *et al.* [46] and Lin *et al.* [42] have discussed cavity enhancement, either through a three-level atom-cavity Λ configuration or an estimate directly from the density of states in the cavity respectively. The resulting enhancements have a $1/L^2$ or $1/L$ dependence [47]. Using the same analysis for our nanocavities, the cavity-enhanced gain coefficient is estimated on order 10^2 larger than the bulk gain coefficient. An alternative first-order approximation would be to use an effective SRS path length interaction approach, such as described in Lin *et al.* [42] and Matsko *et al.* [41], where the Raman gain of the Stokes signal ($\sim \exp(g_c I_c L_c)$) involves the intensity of pump light I_c stored in the cavity, and an effective interaction length L_c described as: $L_c = Q\lambda/2\pi$. For example, the high- Q ($\sim 4.2 \times 10^4$) subwavelength nanocavity described in the next section has an effective interaction length on order 3 mm, a factor of 1.2×10^3 larger than the physical length ($\sim 2.5 \mu\text{m}$) of the cavity.

The next section focuses on the numerical design of specific photonic band gap nanocavities to support Raman amplification and lasing in monolithic silicon.

3. Design and analysis

We consider here a specific photonic band gap nanocavity with linearly aligned missing air holes. The nanocavity is designed numerically with MIT Photonic Bands (MPB) package [48] and the 3D FDTD method [49]. Using MPB, the photonic band structure and the defect resonant frequencies can be obtained. With 3D FDTD method, the defect frequencies, field profiles and Q s can be calculated. The goal of the design is to tune the frequencies of pump mode (f_{pump}) and Stokes mode (f_{Stokes}) with spacing 15.6 THz, corresponding to the optical phonon frequency in monolithic silicon. The wavelengths are also tuned to operate around 1550 nm, with high Q s (on order 10,000 or more) for at least the Stokes mode. The numerical design process is as following: (1) fine-tune the cavity geometry; (2) calculate resonant frequencies f_{pump} and f_{Stokes} with MPB; (3) calculate the lattice constant a based on the frequencies $(f_{pump} - f_{Stokes})(c/a) = 15.6THz$ and calculate the wavelength $\lambda_{pump} = a / f_{pump}$, $\lambda_{Stokes} = a / f_{Stokes}$; (4) calculate Q_{pump} and Q_{Stokes} with 3D FDTD method. The same process can also be used to design nanocavities for anti-Stokes cavity-enhancement, where anti-Stokes generation typically has appreciably lower scattering magnitudes.

The structure investigated is an air-bridge triangular lattice photonic crystal slab with thickness of $0.6a$ and the radius of air holes is $0.29a$, where a is the lattice period. The photonic band gap in this slab for TE-like modes is around $0.25\sim 0.32$ [c/a] in frequency. Two even modes supported in $L3$, $L4$, $L5$ cavities with linearly aligned missing air holes are studied, with which the modal overlap will be maximized. For small cavities such as $L3$ and $L4$, calculated a and λ are large, which will not match the telecommunication applications (around 1550 nm wavelength). For example, in $L3$ cavity, $S_l = 0.15a$, $a = 685$ nm, $\lambda_{pump} = 2266$ nm and $\lambda_{Stokes} = 2568$ nm. Finally, two even modes in single $L5$ cavity are used as the pump and Stokes modes for Raman lasing respectively. Figure 1(a) shows the two defect modal frequencies when a Gaussian impulse is launched at the center of a particular $L5$ cavity.

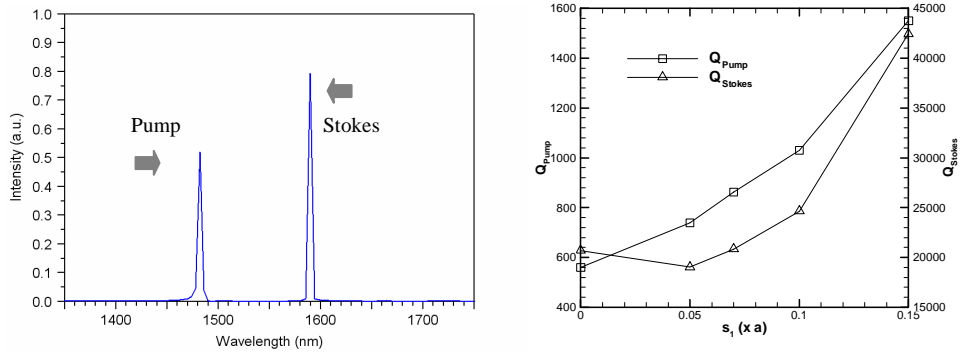


Fig. 1. (a) Resonant frequencies of the pump and Stokes modes within the photonic band gap. (b) Q_{pump} and Q_{Stokes} as a function of shift S_l .

Table 1. Design summary of photonic crystal $L5$ nanocavity for Raman lasing in silicon.

$S_l(x a)$	a (nm)	λ_{pump} (nm)	Q_{pump}	λ_{Stokes} (nm)	Q_{Stokes}
0	456	1592	560	1735.6	20693
0.05	414	1456.4	739	1575.8	19036
0.07	395	1395.7	863	1505	20843
0.10	376	1333.1	1030	1432.4	24642
0.15	342	1215.2	1550	1297.1	42445

Table 1 gives the design summary of fine-tuning the shift S_I of two air-holes at cavity edge. With increasing S_I , the calculated lattice period a decreases and the resonant wavelength λ also decreases due to the constant optical phonon frequency. The quality factors increase because the electric field profile is close to Gaussian function and has less leakage. Figure 1(b) compares the quality factor of pump mode and Stokes mode for different shift of two air holes $S_I = 0 \sim 0.15a$. Q values are obtained by calculating modal transient energy decay with 3D FDTD method: $Q = \omega_0 U / P = -\omega_0 U / (dU/dt)$, where U is the stored energy, ω_0 is the resonant frequency, and $P = -dU/dt$ is the power dissipated. For higher Q nanocavities, a filter diagonalization method [50] can be used. Q_{pump} and Q_{Stokes} are in the order of 10^3 and 10^4 respectively. In comparison with the recently reported work [14, 25, 26], such Q factors can be achievable experimentally, with careful control of the surface roughness and fabrication steps. Higher- Q nanocavities than the results reported here can be achieved by fine-tuning the shift of additional air-holes at cavity edge such as S_2 and S_3 or using double-heterostructure nanocavities without significantly changing the effective modal volume [17]. The designed wavelength of Stokes mode is around 1550 nm and the $L5$ cavity with $S_I = 0.05a$ and $a = 414$ nm is considered in the following calculation.

Figure 2 and Fig. 3 show the electric field profile (E_y) and 2D Fourier transform (FT) spectrum of E_y at the middle of the slab for pump mode and Stokes mode respectively, where the shift S_I of air holes is $0.05a$. Both modes are of even symmetry to maximize the modal overlap. Currently, the modal overlap integral is around 0.5833 between pump mode and Stokes mode due to the small cavity size and the discrete distribution of air holes in PhC slabs. The white circle is the boundary of the light cone. There is a trade-off between the wavelength λ and the quality factor Q . In Fig. 2(b), the FT spectrum of the pump mode contains large components inside the light cone, which indicates large radiative losses and hence lower Q ; the FT spectrum of Stokes mode (Fig. 3(b)), on the other hand, contains much smaller components inside the light cone and corresponds to a higher Q . The higher-order mode (the pump mode in our case) has more serious edge effect (cross-sectional profile differing more significantly from an ideal Gaussian), resulting in a lower Q factor. Figure 4 shows a SEM picture of the specific designed $L5$ nanocavity fabricated at Columbia University.

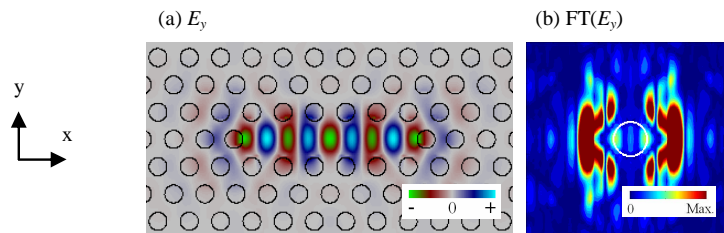


Fig. 2. The electric field profile (E_y) (a) and 2D FT spectrum (b) of pump mode.

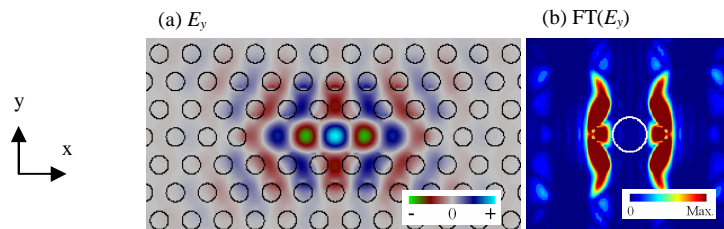


Fig. 3. The electric field profile (E_y) (a) and 2D FT spectrum (b) of Stokes mode.

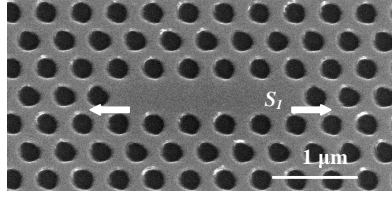


Fig. 4. SEM picture of the PhC $L5$ nanocavity for Raman lasing in silicon.

The estimated modal volume for Stokes mode of the $L5$ cavity is $V_m \sim 0.12 \mu\text{m}^3$. With the calculated Q_{Stokes} at 4.2×10^4 and Q_{pump} at 1550, the resulting Raman lasing threshold in the particular $L5$ nanocavity is conservatively estimated to be on order $344 \mu\text{W}$. This is based on parameters $g_s = 70 \text{ cm/GW}$ and $\xi = 0.5833$. With nanocavities with higher Q_s on order 10^5 [17], the threshold can be further decreased to several to tens of μW . With corresponding silicon microdisk resonators [18, 19], the achievable thresholds are on order several to hundreds of μW depending on specific designs of the microdisks. In comparison with silica-based ultrahigh- Q microspheres and microtoroids, the lower Q in photonic band gap nanocavities is compensated by the 10^3 to 10^4 larger bulk Raman gain in silicon, and the significantly smaller modal volume of the silicon photonic crystal nanocavities. Each of these approaches – the silicon photonic band gap nanocavities, silicon microdisks, or ultra-high Q silica microspheres and microtoroids – supports the push towards achieving ultralow thresholds for Raman lasing on-chip and fundamental nonlinear optics studies.

4. Conclusion

The concept and design of $L5$ photonic band gap nanocavities in two-dimensional photonic crystal slabs for enhancement of stimulated Raman amplification and lasing in monolithic silicon is presented for the first time. Specifically, we describe the numerical design of a high quality factor and small modal volume nanocavity that supports the required pump-Stokes modal spacing in silicon, with ultralow lasing thresholds. This concept and design supports the push towards on-chip all-optical signal amplification and lasing in monolithic silicon.

Acknowledgments

This work is supported by the Columbia Initiative in Science and Engineering for Nanophotonics.